Sampling vacancy configurations with large relaxations using Smart Darting: supplemental material

D. Tanguy[1, *]

[1] *Univ Lyon, Université Claude Bernard Lyon 1, CNRS, Institut Lumière Matière, F-69622, VILLEURBANNE, France*

(Dated: February 14, 2024)

I. EXAMPLE OF A VACANCY TRAJECTORY

The vacancy trajectory in Fig. 1 was obtained by an MCMC simulation with Smart Darting moves at T=400 K and under 3% strain perpendicular to the grain boundary plane. The vacancy performs a one dimensional random walk along the tilt axis before leaving the GB and doing a 3D random walk in the perfect crystal before entering again the GB, performing another 1D random walk and finally leaving the GB again. The trajectory was originally obtained with periodic boundary conditions and was "unfolded" for the figure.

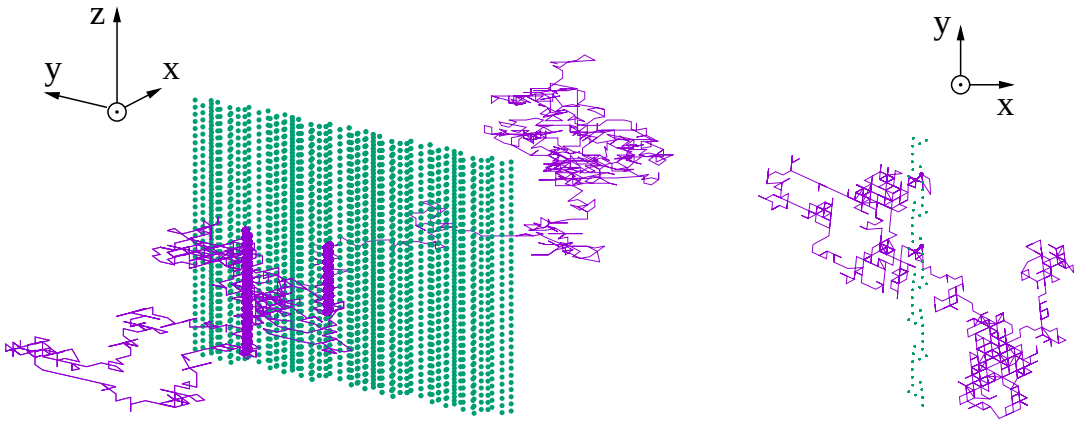

Figure 1. A trajectory (purple) of a single vacancy along and out of the $\Sigma 33\{5\bar{5}4\}[110]$, under 3% strain perpendicular to the interface, in Al. The green dots are the lattice sites of the core region of the GB. Left is a 3D view, right is the same trajectory projected in the (x,y) plane, perpendicular to the tilt axis.

II. VACANCY SEGREGATION ENERGY PROFILES

The vacancy segregation energy profiles in figure 2 are obtained by removing a particle sequentially on every lattice site in the vicinity of the interface, starting from the minimum energy structure, and minimizing the energy. They are coherent with the maps given in the paper. The energies are not necessarily the same as the ones found by the Monte Carlo simulation because there can be local minima separated by barriers. In the Monte CArlo simulation, the system is thermalized and the topologies are periodically searched after the energy is minimized. In the absence of external strain, the most stable vacancy configurations are the same between the two methods, for single vacancies, apart from minor differences in relaxations and the energy differences are small. Sometimes, the true minimum is separated by the starting configuration by an energy barrier (for example, in the $\Sigma 33$ under strain in Fig. 3 in the paper or in the case of divacancies in Fig. 5 below). In this case the relevant configuration is missed by the direct minimization but can be found by the Monte Carlo simulation either because the barrier is crossed by the Δu moves or found by the NEB searches (as an intermediate minimum between the end points).

* dome.tanguy@univ-lyon1.fr

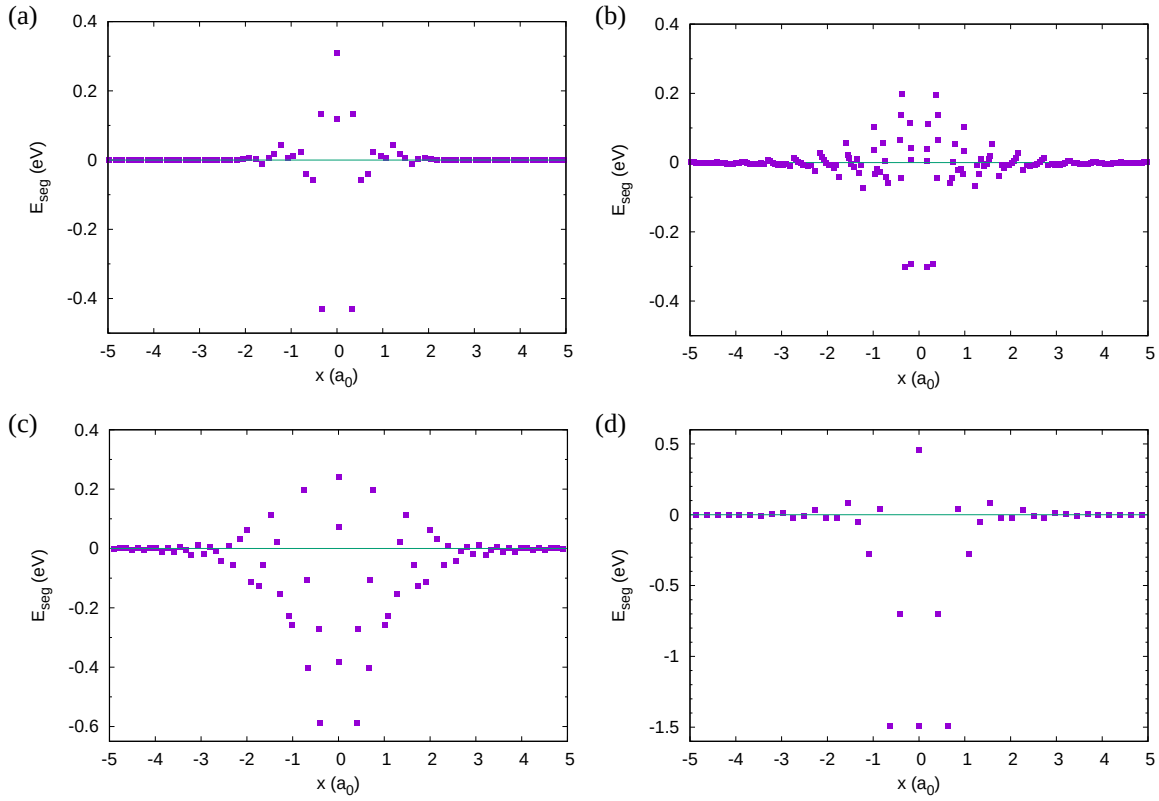

Figure 2. Vacancy segregation energy profiles, perpendicular to the interface plane: (a) $\Sigma 13\{320\}[001]$ and (b) $\Sigma 33\{5\bar{5}4\}[110]$ in Al and (c) $\Sigma 29\{730\}[001]$ and (d) $\Sigma 9\{1\bar{1}4\}[110]$ in bcc Fe.

III. DIVACANCY SIMULATIONS IN FE

Figure 3 gives additional information about the behavior of divacancies by reporting simulations done on $\Sigma 29\{730\}[001]$ and $\Sigma 9\{1\bar{1}4\}[110]$ symmetrical tilt boundaries in bcc Fe (T=300 K). In figure 3(a) ($\Sigma 29$), a simulation is started with two vacancies far apart. The algorithm progressively learns the topologies where the vacancies are closer and closer until d=1 and the energy decreases by more than 1 eV (the energy shown on the graph corresponds to the energy of the topologies visited, not to the energy of the system, see paper). Then the system remains in this configuration i.e. the divacancy is not split at this temperature and no migration of the divacancy by Δu moves was found. On the opposite, in figure 3(b) ($\Sigma 9$), the system is constructed with the vacancies separated by $\sqrt{(2)}\ a_0$ (the minimal distance along the tilt axis). The vacancies split during the simulation and seldom visit the configuration $d = \sqrt{(2)}\ a_0$ again, in agreement with a repulsive interaction at T=0 of 60 meV.

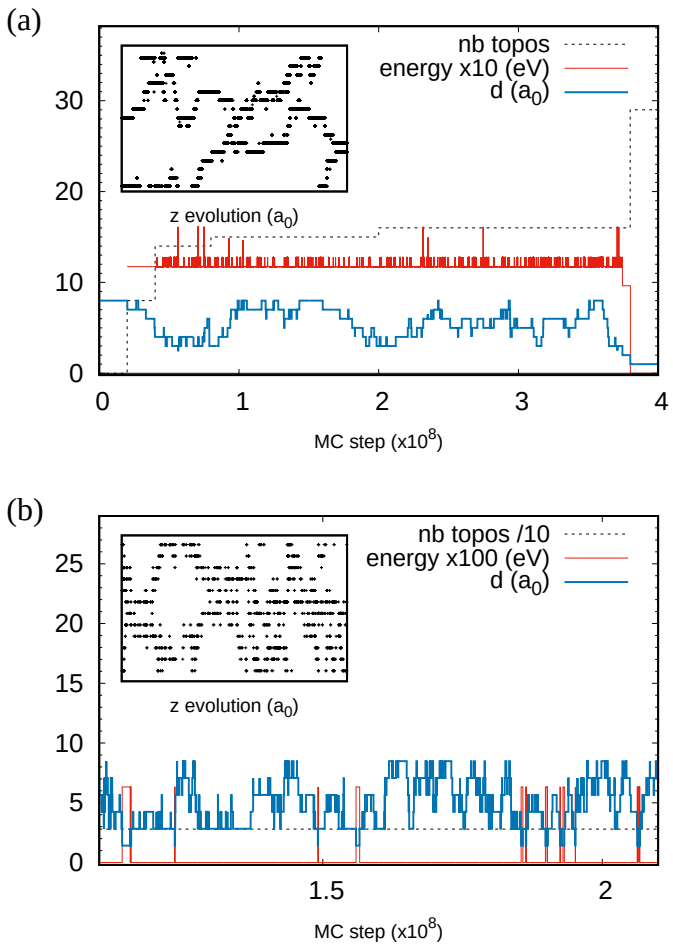

Figure 3. Evolution of the distance between the vacancies, the energy of the topology visited and the number of topologies detected along the Markov chain for a system containing two vacancies: (a) $\Sigma 29\{730\}[001]$ and $\Sigma 9\{1\overline{1}4\}[110]$ in bcc Fe. The position in z (the tilt axis direction) is shown on the insert.

IV. OTHER INFORMATION CONCERNING INTERGRANULAR DIVACANCIES IN AL

In this section additional information concerning divancies in Al are given: the number of topologies found, the number of topologies visited and the structure and position of the lowest energy configurations found. Figure 4a concerns the $\Sigma 33\{554\}[110]$ symmetric tilt grain boundary in Al. The structures of low energy are shown in the main article. The lowest energy configuration corresponds to two vacancies aligned along the tilt axis, in first neighbor position and on the sites where the segregation energy of the single vacancy is the most favorable (-0.29 eV). This structure is taken as the reference for the energies on figure 4a. The energy that has to be spent to break the divacancy (the binding energy) but leave the vacancies on the same type of site is 0.28 eV. The number of topologies extracted is 45. Essentially, only the topologies with energies 0, 0.28 and 0.52 were visited, at T=600 K. For this grain boundary the configuration of the divacancy is intuitive but it is not always the case, for example in the $\Sigma 9\{221\}[110]$ detailed below.

Four low energy configurations for divacancies in the $\Sigma 9\{221\}[110]$ symmetrical tilt grain boundary in Al are shown in figure 5. The three first are for vacancies in first neighbor position. The divacancy is split in the the last one. Configurations (a) and (b) are connected by low barriers (0.3 eV / 0.2 eV). Configuration (a) was found by Δu moves from configuration (b). Note that both vacancies occupy different lattice sites. Configuration (c) is a variant from configuration (b) where only the displacements are different. They are also connected by low barriers (0.12 eV / 0.16 eV). Starting a simulation from configuration (c) (constructed by hand), the system made a transition to configuration (b) by Δu moves. During the search for topologies, the algorithm takes into consideration not only the transitions where a vacancy is exchanged with one of its neighbors, but also the existence of additional configurations which differ

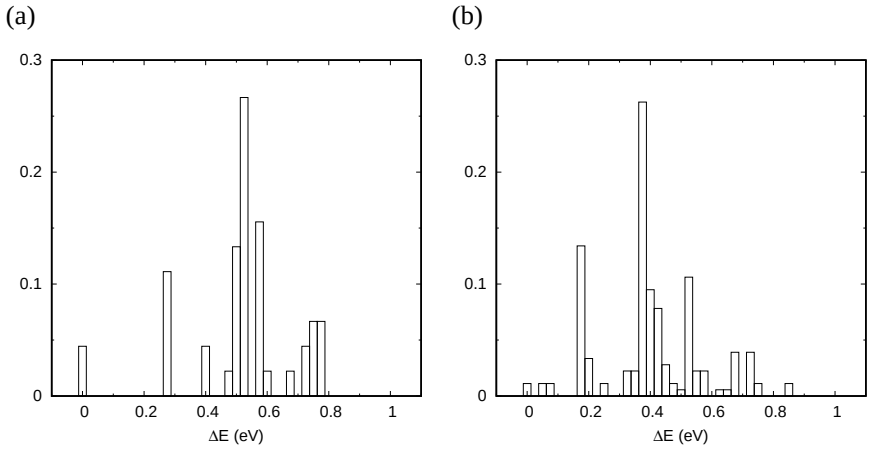

Figure 4. Histograms of the energies of the different topologies explored by the method in the case of the (a) Σ33{554}[110] and (b) Σ9{221}[110] symmetrical tilt grain boundaries in Al.

by their displacements only. The NEB calculates the barriers for all these transitions and the appropriate topologies are extracted. About 50 topologies were extracted during the Monte Carlo run. A temperature of 400 K is high enough to observe the displacement of the divacancy along the tilt axis, which means that Smart Darting is efficient. The distribution of the energies is shown in Fig. 4b. The last configuration (d) is connected to (b) with barriers 0.66 eV / 0.55 eV. Such transitions occur only by Smart Darting moves because the barriers are too high to be crossed only by Δu moves at the low temperatures of interest for the clustering problem.

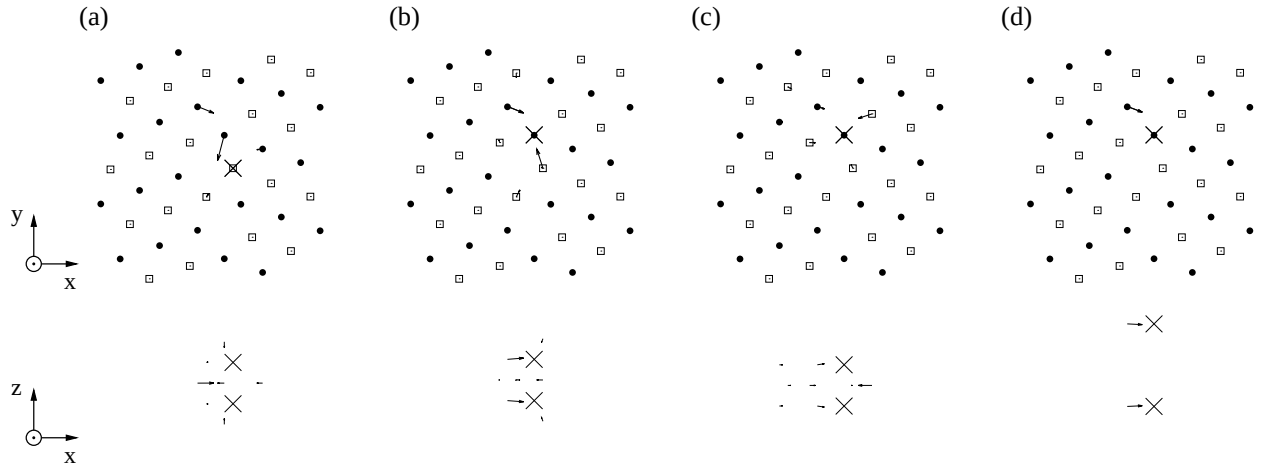

Figure 5. Divacancy configurations of low energy in the Σ9{221}[110] symmetrical tilt grain boundaries in Al. The energies are (a) 0 eV, (b) 0.1 eV, (c) 0.06 eV and (d) 0.2 eV.

In complement, the segregation energies of an isolated vacancy in this grain boundary are given in Fig. 6.

V. ELASTIC DIPOLE TENSOR FROM KANZAKI FORCES: CONVERGENCE

[1] E. Clouet, C. Varvenne, and T. Jourdan, Comp. Mat. Sci. **147**, 49 (2018).

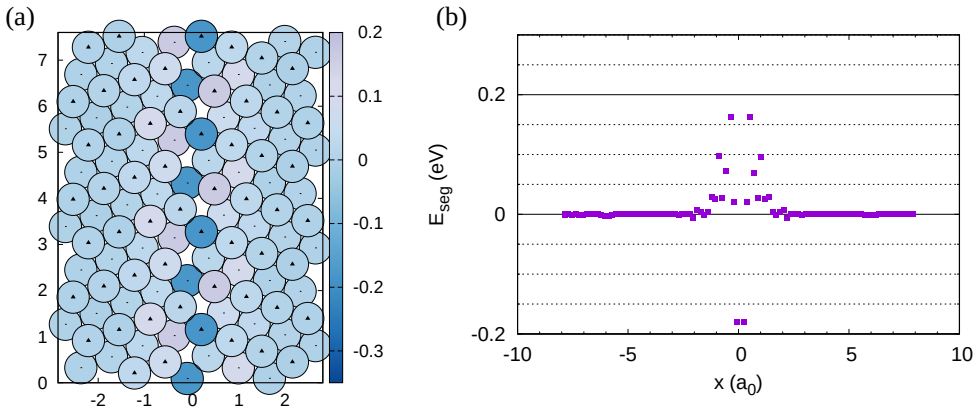

Figure 6. Vacancy segregation energy for Σ9{221}[110] symmetrical tilt grain boundaries in Al: (a) map and (b) profiles.

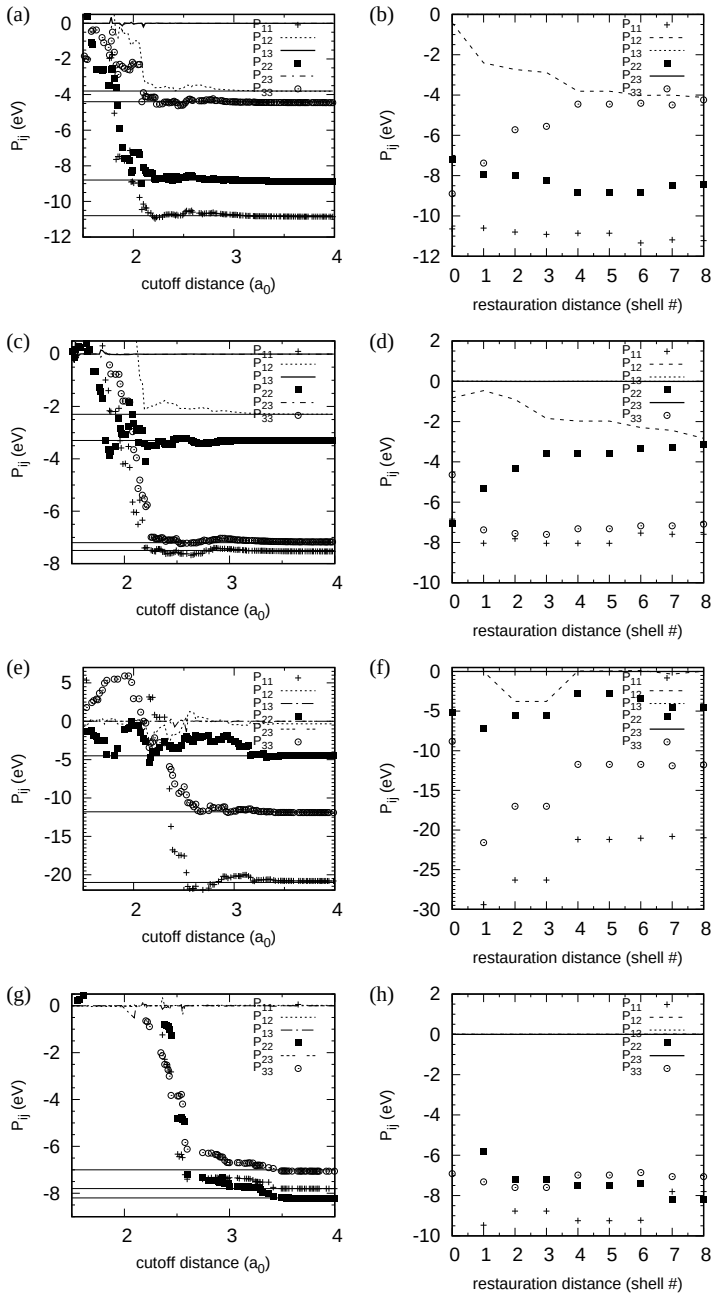

Figure 7. Elastic dipole tensor from Kanzaki forces: convergence. Symmetrical tilt grain boundaries: (a,b) Σ13{320}[100], (c,d) Σ33{554}[110] in Al and (e,f) Σ29{730}[100], (g,h) Σ9{114}[110] in bcc Fe. The graphs give the variation of the tensor components as a function of the cutoff radius in the sum $P_{jk} = \sum_q F_j^q a_k^q$, where F is the Kanzaki force at the lattice site a [1] and the influence of the restoration radius. Constant values means that all the remaining relaxations are harmonic [1].